

# DIRECT AEROACOUSTIC AND AERODYNAMIC SIMULATION OF MULTI-HOLE ENGINE LINERS

Jingmei Liu \*, and Lyle N. Long†  
Department of Aerospace Engineering  
The Pennsylvania State University  
University Park, PA 16802  
lnl@psu.edu

## Abstract

This paper presents a new method to simulate the aeroacoustics and aerodynamics of engine liners. The method is based on the nonlinear disturbance equations (NLDE). First a steady state flow field is computed by a standard CFL code (or analytically) and then the NLDE is used to simulate the perturbations. Numerically it is fourth order accurate in space and time. Thompson characteristic boundary conditions are applied to introduce acoustic waves at the inlet boundary of the duct. A typical engine liner unit with three holes on the face sheet is studied with and without the influence of a mean flow. The results show the interaction between the holes and their contributions to the acoustics in the duct. This study supplies a better understanding of the mechanism of engine liner aeroacoustics. Parallel computers are a necessity for this compute-intensive problem.

## Introduction

Aircraft duct liners for turbofan engines need to be safe, durable, and efficient, in addition to being able to reduce radiated noise. This is especially difficult when trying to suppress broadband noise from advanced high-bypass-ratio engines or for discrete frequency fan noise over a wide range of engine power settings. Optimal liners will have varying hole sizes, hole spacings, cavity depths, etc. These designs usually rely upon extensive experimental tests, which are quite time consuming and costly. These tests usually need to be conducted at full-scale, since nonlinear effects prohibit scaling the results. Acoustic treatment design methods are strongly dependent on empirical and semi-empirical methods.

Until recently only frequency-domain methods had been used for the prediction of sound propagation in

acoustically treated ducts,<sup>10</sup> as well as for the extraction of the impedance (inverse problem) of the material.<sup>14, 15</sup> However, frequency-domain methods,<sup>1</sup> unlike the time-domain methods, can only solve for one frequency at a time. When broadband frequency response and nonlinear effects are important, time-domain methods are more suitable. Recent research has shown that time-domain numerical methods<sup>7, 8, 12</sup> may be suitable for evaluating different liner designs.

Until recently little research had been done on the effects of high sound pressure levels on propagation through liners, a problem in nonlinear acoustics.<sup>2</sup> A better understanding of flow mechanisms around liner structures would be very useful for improving the design methods and the impedance models. Recently developed parallel methods and computers now make solving nonlinear liner problems possible. Direct aeroacoustic and aerodynamic simulations can be used to study waves propagating in the duct in a nonuniform flow, including the effects of hole-hole interactions and boundary layers.

In this paper, a three dimensional direct aeroacoustic and aerodynamic solver is described which simulates multi-hole liners. The important nonlinearities, and the viscous and grazing flow effects, are considered simultaneously.

This research is related to the research being performed in the NASA Langley flow-impedance tube facility<sup>9</sup> shown in fig. 1 This apparatus has a 51 x 51 mm cross section and is designed to produce a controlled aeroacoustic environment with a Mach number up to 0.6 over a test specimen length of 41 cm. Four 120-W phase-matched acoustic drivers generate signals over a frequency range of 0.3-3.0 kHz, with sound pressure level up to 155 dB at the test specimen leading edge. Acoustic waves propagate from left to right, across the surface of the test specimen, and into a termination section designed to minimize reflections over the frequency range of interest. Our numerical simulation models a typical configuration. The numerical solution will be compared with experimental data from this facility in the future.

---

\*Research Associate

†Professor, Associate Fellow AIAA

<sup>0</sup>Copyright ©1998 by the American Institute of Aeronautics and Astronautics, Inc. with Permission.

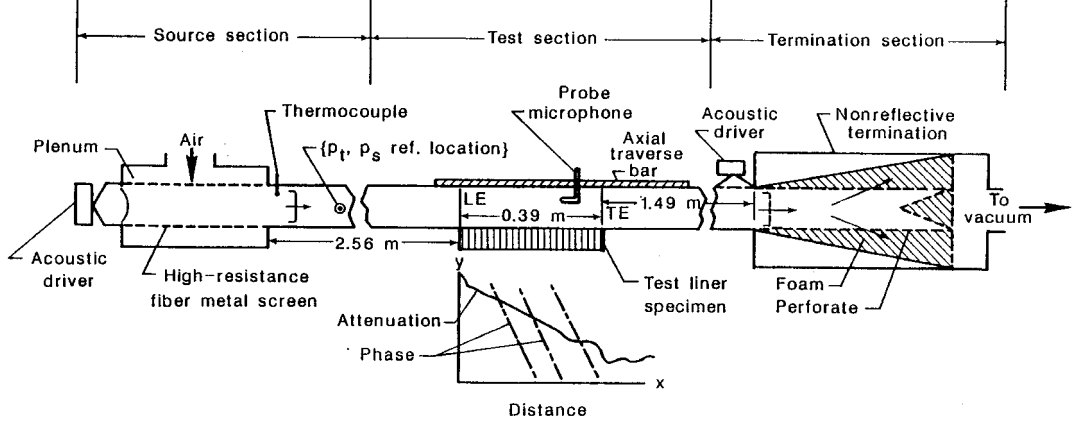


Figure 1: NASA Langley flow-impedance tube facility<sup>9</sup>

## Nonlinear Disturbance Equations (NLDE)

The methodology used here is based on the nonlinear disturbance equations, which is a newly developed numerical method.<sup>4</sup> The general Navier-Stokes equations in a Cartesian coordinate system are:

$$\frac{\partial q}{\partial t} + \frac{\partial F}{\partial x} + \frac{\partial G}{\partial y} + \frac{\partial H}{\partial z} = \frac{\partial R}{\partial x} + \frac{\partial S}{\partial y} + \frac{\partial E}{\partial z} \quad (1)$$

where  $F$ ,  $G$ , and  $H$  are the inviscid terms and  $R$ ,  $S$ ,  $E$  are the viscous terms. The results presented here will all be inviscid. The flow field is split into a mean and a fluctuating part:

$$q(\vec{x}, t) = q_o(\vec{x}) + q'(\vec{x}, t) \quad (2)$$

where

$$q = \begin{Bmatrix} \rho \\ \rho u \\ \rho v \\ \rho w \\ e \end{Bmatrix} \quad (3)$$

and

$$q_o = \lim_{T \rightarrow \infty} \frac{1}{T} \int_{t_0}^{t_0+T} q(t) dt \quad (4)$$

Substituting equation (2) into (1) and rearranging results in the nonlinear disturbance equations (NLDE):

$$\frac{\partial q'}{\partial t} + \frac{\partial F'}{\partial x} + \frac{\partial G'}{\partial y} + \frac{\partial H'}{\partial z} = Q \quad (5)$$

Where

$$q' = \begin{Bmatrix} \rho' \\ \rho_o u' + \rho' u_o + \rho' u' \\ \rho_o v' + \rho' v_o + \rho' v' \\ \rho_o w' + \rho' w_o + \rho' w' \\ e' \end{Bmatrix} \quad (6)$$

On the left hand side of the NLDE are terms related to the perturbation properties and the cross terms (linear and nonlinear), whereas the right hand side contains strictly mean flow terms.

The convective fluxes involving the perturbation quantities  $F'$ ,  $G'$  and  $H'$  are given as

$$F' = \begin{Bmatrix} \rho_o u' + \rho' u_o + \rho' u' \\ \rho' u_o^2 + 2\rho_o u_o u' + p' \\ + 2\rho' u' u_o + (\rho_o + \rho') u' u' \\ \rho_o u_o v' + \rho_o v_o u' + \rho' u_o v_o \\ + \rho' v' u_o + \rho' u' v_o + (\rho_o + \rho') u' v' \\ \rho_o u_o w' + \rho_o w_o u' + \rho' u_o w_o \\ + \rho' w' u_o + \rho' u' w_o + (\rho_o + \rho') u' w' \\ u'(e_o + p_o) + (u_o + u')(e' + p') \end{Bmatrix} \quad (7)$$

$$G' = \left\{ \begin{array}{l} \rho_o v' + \rho' v_o + \rho' v' \\ \rho_o v_o u' + \rho_o u_o v' + \rho' u_o v_o \\ + \rho' v' u_o + \rho' u' v_o + (\rho_o + \rho') u' v' \\ \rho' v_o^2 + 2\rho_o v_o v' + p' \\ + 2\rho v' v_o + (\rho + \rho') v' v' \\ \rho_o v_o w' + \rho_o w_o v' + \rho' v_o w_o \\ + \rho' w' v_o + \rho' v' w_o + (\rho_o + \rho') v' w' \\ v'(e_o + p_o) + (v_o + v')(e' + p') \end{array} \right\} \quad (8)$$

$$H' = \left\{ \begin{array}{l} \rho_o w' + \rho' w_o + \rho' w' \\ \rho_o w_o u' + \rho_o u_o w' + \rho' u_o w_o \\ + \rho' w' u_o + \rho' u' w_o + (\rho_o + \rho') u' w' \\ \rho_o w_o v' + \rho_o v_o w' + \rho' w_o v_o \\ + \rho' v' w_o + \rho' v' w_o + (\rho_o + \rho') v' w' \\ \rho' w_o^2 + 2\rho_o w_o w' + p' \\ + 2\rho w' w_o + (\rho_o \rho') w' w' \\ w'(e_o + p_o) + (w_o + w')(e' + p') \end{array} \right\} \quad (9)$$

The mean flow source term  $Q$  is time independent:

$$Q = - \left( \frac{\partial F_o}{\partial x} + \frac{\partial G_o}{\partial y} + \frac{\partial H_o}{\partial z} \right) + \frac{\partial R_o}{\partial x} + \frac{\partial S_o}{\partial y} + \frac{\partial E_o}{\partial z} \quad (10)$$

If the NLDE is time averaged, it becomes the Reynolds-averaged Navier-Stokes equation, where the Reynold's stresses are on the left hand side. Thus, for a laminar flow  $Q = 0$ .

We seek a solution of the perturbation variables  $q'$  with a known mean flow field, which can be obtained from existing well-developed CFD codes (e.g. CFL3D<sup>6</sup>) or analytically, for steady flow. This methodology allows us to use the most effective algorithms for the steady and unsteady portions of field, respectively.<sup>3</sup> It also minimizes round-off error since we are only computing perturbations. We can even use different grids for the steady and unsteady solution. More discussion on this new method is in the reference.<sup>4</sup>

## Characteristic Boundary Conditions for NLDE

The boundary conditions for the NLDE are developed by applying Thompson's characteristic method<sup>13</sup> to the nonlinear disturbance equations. Instead of using the conservative form of the equations, the boundary conditions are derived based on the nonconservative form:

$$\frac{\partial \rho}{\partial t} + \rho \frac{\partial u_j}{\partial x_j} + u_j \frac{\partial \rho}{\partial x_j} = 0 \quad (11)$$

$$\frac{\partial p}{\partial t} + \gamma p \frac{\partial u_j}{\partial x_j} + u_j \frac{\partial p}{\partial x_j} - VIS_p = 0 \quad (12)$$

$$\rho \frac{\partial u_i}{\partial t} + \rho u_j \frac{\partial u_i}{\partial x_j} + \frac{\partial p}{\partial x_j} - VIS_{vel} = 0 \quad (13)$$

Here  $VIS_p$  and  $VIS_{vel}$  are viscous terms. Substituting equation (2) into (11) - (13) and rearranging gives the boundary conditions in nonlinear perturbation form:

$$\begin{aligned} \frac{\partial \rho'}{\partial t} + (\rho_o + \rho') \frac{\partial u_j'}{\partial x_j} + (u_{oj} + u_j') \frac{\partial \rho'}{\partial x_j} = \\ - (\rho' \frac{\partial u_{oj}}{\partial x_j} + u_j' \frac{\partial \rho_o}{\partial x_j}) - (\rho_o \frac{\partial u_{oj}}{\partial x_j} + u_{oj} \frac{\partial \rho_o}{\partial x_j}) \end{aligned} \quad (14)$$

$$\begin{aligned} \frac{\partial p'}{\partial t} + \gamma(p_o + p') \frac{\partial u_j'}{\partial x_j} + (u_{oj} + u_j') \frac{\partial p'}{\partial x_j} = \\ - (\gamma p' \frac{\partial u_{oj}}{\partial x_j} + u_j' \frac{\partial p_o}{\partial x_j}) - (\gamma p_o \frac{\partial u_{oj}}{\partial x_j} + u_{oj} \frac{\partial p_o}{\partial x_j}) \\ + VIS_p \end{aligned} \quad (15)$$

$$\begin{aligned} \frac{\partial u_i'}{\partial t} + (u_{oj} + u_j') \frac{\partial u_i'}{\partial x_j} + \frac{1}{\rho_o + \rho'} \frac{\partial p'}{\partial x_i} = \\ - (u_j' \frac{\partial u_{oi}}{\partial x_j} + \frac{1}{\rho_o + \rho'} \frac{\partial p_o}{\partial x_i}) - u_{oj} \frac{\partial u_{oi}}{\partial x_j} \\ + VIS_{vel} \end{aligned} \quad (16)$$

Here we apply a characteristic analysis to the perturbation variables and move the mean flow terms to the right hand side, which is different than the approach employed by others. Now considering a boundary located at  $x = x_o$  and using the characteristic analysis<sup>13</sup> to modify the hyperbolic terms of Eqs. (14) - (15) corresponding to waves propagating in the  $x$  direction, we can recast this system as:

$$\begin{aligned} \frac{\partial \rho'}{\partial t} + \frac{1}{c^2} [L_2 + \frac{1}{2}(L_1 + L_5)] + (\rho_o + \rho') \left( \frac{\partial v'}{\partial y} + \frac{\partial w'}{\partial z} \right) \\ + (v_o + v') \frac{\partial \rho'}{\partial y} + (w_o + w') \frac{\partial \rho'}{\partial z} = - [\rho' \left( \frac{\partial u_o}{\partial x} + \frac{\partial v_o}{\partial y} + \right. \\ \left. \frac{\partial w_o}{\partial z} \right) + (u' \frac{\partial \rho_o}{\partial x} + v' \frac{\partial \rho_o}{\partial y} + w' \frac{\partial \rho_o}{\partial z})] - [\rho_o \left( \frac{\partial u_o}{\partial x} + \right. \\ \left. \frac{\partial v_o}{\partial y} + \frac{\partial w_o}{\partial z} \right) + (u_o \frac{\partial \rho_o}{\partial x} + v_o \frac{\partial \rho_o}{\partial y} + w_o \frac{\partial \rho_o}{\partial z})] \end{aligned} \quad (17)$$

$$\begin{aligned}
\frac{\partial p'}{\partial t} + \frac{1}{2}(L_1 + L_5) + \gamma(p_0 + p')\left(\frac{\partial v'}{\partial y} + \frac{\partial w'}{\partial z}\right) + \\
(v_0 + v')\frac{\partial p'}{\partial y} + (w_0 + w')\frac{\partial p'}{\partial z} = -[\gamma p'\left(\frac{\partial u_0}{\partial x} + \right. \\
\left. \frac{\partial v_0}{\partial y} + \frac{\partial w_0}{\partial z}\right) + (u'\frac{\partial p_0}{\partial x} + v'\frac{\partial p_0}{\partial y} + w'\frac{\partial p_0}{\partial z})] \\
-[\gamma p_0\left(\frac{\partial u_0}{\partial x} + \frac{\partial v_0}{\partial y} + \frac{\partial w_0}{\partial z}\right)(u_0\frac{\partial p_0}{\partial x} + \\
v_0\frac{\partial p_0}{\partial y} + w_0\frac{\partial p_0}{\partial z})] + VIS_p \quad (18)
\end{aligned}$$

$$\begin{aligned}
\frac{\partial u'}{\partial t} + \frac{1}{2(\rho_0 + \rho')c}(L_5 - L_1) + (v_0 + v')\frac{\partial u'}{\partial y} + \\
(w_0 + w')\frac{\partial u'}{\partial z} = -[u'\frac{\partial u_0}{\partial x} + v'\frac{\partial u_0}{\partial y} + w'\frac{\partial u_0}{\partial z}] \\
-[(u_0\frac{\partial u_0}{\partial x} + v_0\frac{\partial u_0}{\partial y} + w_0\frac{\partial u_0}{\partial z}) + \frac{1}{\rho_0 + \rho'}\frac{\partial p_0}{\partial x} \\
+ VIS_u \quad (19)
\end{aligned}$$

$$\begin{aligned}
\frac{\partial v'}{\partial t} + L_3 + (v_0 + v')\frac{\partial v'}{\partial y} + (w_0 + w')\frac{\partial v'}{\partial z} + \\
\frac{1}{\rho_0 + \rho'}\frac{\partial p'}{\partial y} = -[u'\frac{\partial v_0}{\partial x} + v'\frac{\partial v_0}{\partial y} + w'\frac{\partial v_0}{\partial z}] \\
-[(u_0\frac{\partial v_0}{\partial x} + v_0\frac{\partial v_0}{\partial y} + w_0\frac{\partial v_0}{\partial z}) + \frac{1}{\rho_0 + \rho'}\frac{\partial p_0}{\partial y} \\
+ VIS_v \quad (20)
\end{aligned}$$

$$\begin{aligned}
\frac{\partial w'}{\partial t} + L_4 + (v_0 + v')\frac{\partial w'}{\partial y} + (w_0 + w')\frac{\partial w'}{\partial z} + \\
\frac{1}{\rho_0 + \rho'}\frac{\partial p'}{\partial z} = -[u'\frac{\partial w_0}{\partial x} + v'\frac{\partial w_0}{\partial y} + w'\frac{\partial w_0}{\partial z}] \\
-[(u_0\frac{\partial w_0}{\partial x} + v_0\frac{\partial w_0}{\partial y} + w_0\frac{\partial w_0}{\partial z}) + \frac{1}{\rho_0 + \rho'}\frac{\partial p_0}{\partial z} \\
+ VIS_w \quad (21)
\end{aligned}$$

where the  $L_i$ 's are the amplitudes of characteristic waves associated with each characteristic velocity  $\lambda_i$ . These are given by:

$$\lambda_1 = (u_0 + u') - c \quad (22)$$

$$\lambda_2 = \lambda_3 = \lambda_4 = u_0 + u' \quad (23)$$

$$\lambda_5 = (u_0 + u') + c \quad (24)$$

where  $c$  is the speed of sound:

$$c^2 = \gamma \frac{p_0 + p'}{\rho_0 + \rho'} \quad (25)$$

$\lambda_1$  and  $\lambda_5$  are the speed of acoustic waves moving in the negative and positive  $x$  direction;  $\lambda_2$  is the convection velocity (the speed at which entropy waves will travel) while  $\lambda_3$  and  $\lambda_4$  are the velocities at which  $v$  and  $w$  are advected in the  $x$  direction. The  $L_i$ 's are given by:

$$L_1 = \lambda_1 \left[ \frac{\partial p'}{\partial x} - (\rho_0 + \rho')c \frac{\partial u'}{\partial x} \right] \quad (26)$$

$$L_2 = \lambda_2 \left( c^2 \frac{\partial \rho'}{\partial x} - \frac{\partial p'}{\partial x} \right) \quad (27)$$

$$L_3 = \lambda_3 \frac{\partial v'}{\partial x} \quad (28)$$

$$L_4 = \lambda_4 \frac{\partial w'}{\partial x} \quad (29)$$

$$L_5 = \lambda_5 \left[ \frac{\partial p'}{\partial x} + (\rho_0 + \rho')c \frac{\partial u'}{\partial x} \right] \quad (30)$$

We have shown here the characteristic boundary conditions in the  $x$  direction. The equations for the  $y$  and  $z$  directions are derived in a similar manner. For edges and corners in three dimensions the equations for the various directions are combined into one approximate equation.

This type of boundary condition treatment also allows one to easily introduce a disturbance at the incoming boundary by deriving an expression for one of the incoming characteristics with a source term. At the outflow boundaries, the boundary conditions are essentially non-reflecting.

## Numerical Method and Parallel Methodology

The NLDE are cast in a generalized coordinate system and solved numerically using a finite difference scheme. The discretized equations are solved in a time accurate manner by taking advantage of computational aeroacoustics (CAA) methods. The spatial flux derivatives are calculated using seven point stencils of the fourth order optimized Dispersion Relation Preserving (DRP) scheme of Tam and Webb.<sup>11</sup> The time integration is a fourth order accurate Runge-Kutta method.

Efficient computing performance is achieved by using a three dimensional domain decomposition strategy and parallel computers. The code is written in Fortran 77 plus Message Passing Interface (MPI)<sup>5</sup> and is scalable in three dimensions. The multi-hole liner configuration is too complicated for a multi-block grid. In order to make the code scalable and flexible, a three dimensional single-block grid is used. The whole computational domain is

divided into many three dimensional zones. The grid points are evenly distributed across each processor.

The NLDE solver is implemented portably on parallel computers, such as the IBM SP2 (e.g. Penn State, NPACI, MHPCC), SGI Power Challenge and Pentium II Cluster. A comparison of code performance for the NLDE code run on various machines is shown in Fig. 2. While a 24-processor IBM SP2 is 8.4 times faster than 8 Pentium II's (266 MHz and Fast Ethernet) networked together, the SP2 costs roughly 14 times more than the PC cluster. Fig. 3 gives the wall clock time for the NLDE code with 1.86 million grid points using varying number of processors. A 64-processor SP2 is roughly 2.6 time faster than a 16-processor SP2 (when problem size is kept fixed).

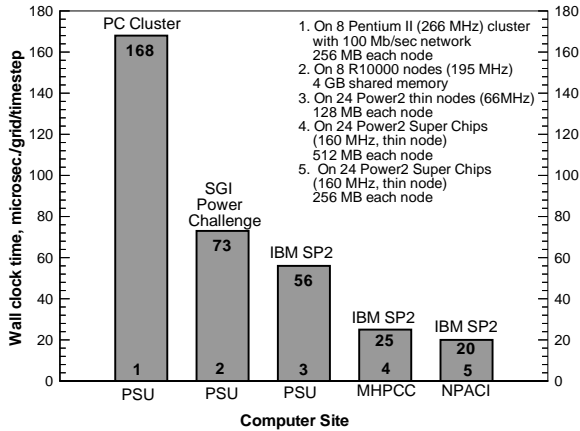


Figure 2: Timings of NLDE code on several parallel computers

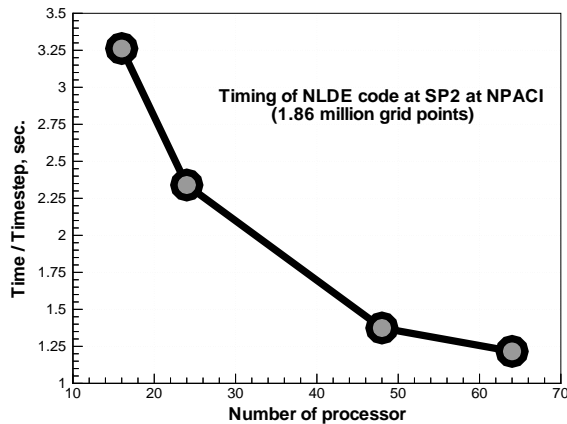


Figure 3: Timings of NLDE code on SP2

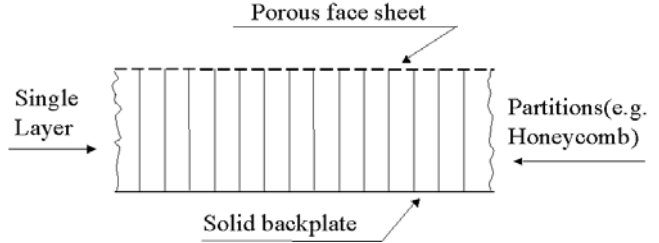


Figure 5: schematic of a single layer liner

## Results and Discussions

The configuration of the NASA Langley flow-impedance tube is depicted in fig. 1. A typical single layer liner specimen is shown in fig. 5. The test segment consists of three parts, the porous face sheet, the partitions (e.g. honeycomb) and solid backplate. Our preliminary approach to this application is to simulate one of the honeycomb cavities. As shown in fig. 4, it has a three-hole face sheet, a rectangular cavity and a backplate. Similar to the flow-impedance tube facility, a duct flow with inlet boundary layer is set up over the face sheet. An acoustic wave is input at the upstream boundary of the duct.

The liner wall and duct wall are treated as solid walls using Thompson's characteristic wall boundary condition, which was discussed earlier. At the inlet boundary, characteristic boundary conditions allow both the incoming and outgoing waves. The presence of the liner causes the generation of additional modes in the duct that can propagate in both directions. The condition for the inlet boundary to be nonreflective yet at the same time a source plane is achieved by deriving an expression for one of the incoming characteristics with a source term, here we have:

$$L_5 = 2\sqrt{2}p_{ref}10^{A/20}\omega\cos\omega t \quad (31)$$

instead of  $L_5 = 0$ . This term enables us to generate a plane wave at a circular frequency of  $\omega$  and a sound pressure level of  $A$  dB. Here  $p_{ref}$  is the reference pressure. Nonreflective characteristic boundary conditions are applied at the exit.

The computational grid for this problem is  $121 \times 127 \times 153$ . There are  $11 \times 11$  grid points covering each hole on the face sheet.

Two sets of numerical simulations are performed and discussed. The first case has a plane pressure wave coming in from the upstream boundary (left side in fig. 4). The amplitude of the wave is 23.5 PA and its frequency is 2720 Hz. There is no mean flow in the duct. The second case has the same acoustic wave but there is a mean flow of Mach number 0.1 through the duct. The profile of the mean flow is obtained by using a Blasius laminar boundary layer solution. The thickness of the

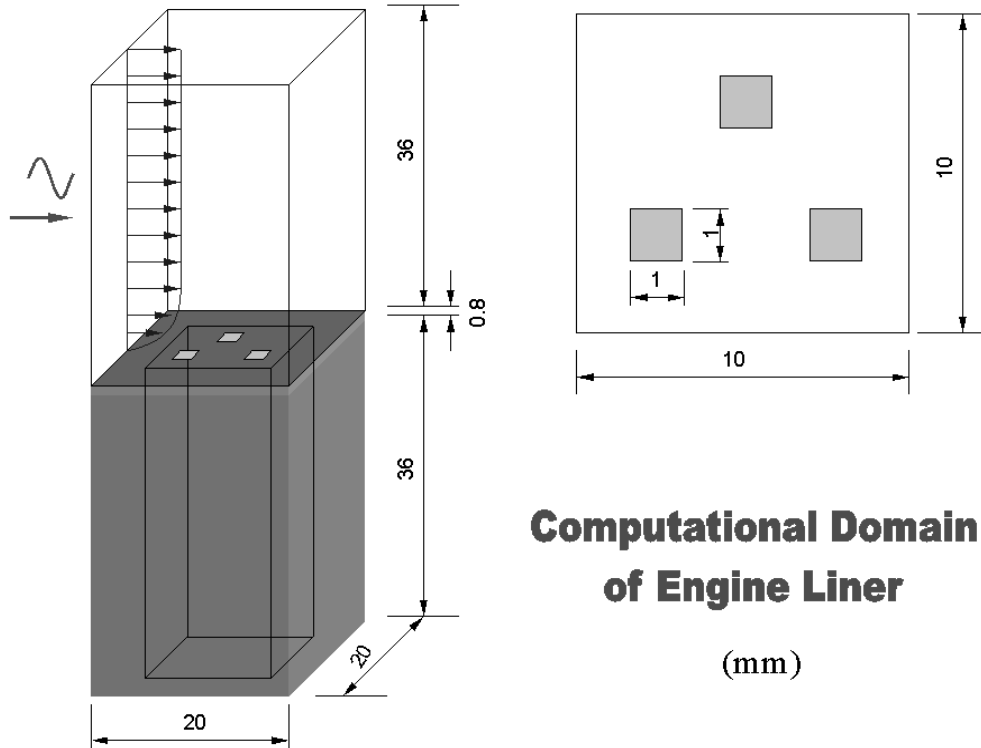


Figure 4: Computational domain of engine liner

boundary layer at the inlet boundary of the computational domain is evaluated by the distance from the inlet of the test rig in fig. 1 It is acknowledged that this is only an approximate representative of the inlet boundary layer. In future work, CFL3D will be used to supply the background flow. In this paper, we will show interaction between the holes on the face sheet and the effect of the boundary layer over the holes.

Fig. 6 to fig. 9 show the results for the case without mean flow at four different times, fig. 10 to fig. 13 show the results for the case with mean flow.  $T$  is the time period of the wave. In each figure the plane wave enters from the left boundary and there are three instantaneous acoustic pressure contour plots. The left one is the horizontal slice on the top of face sheet which shows the perturbation interactions between holes on the duct wall. The shape of the plane wave is changed greatly near the holes and the pattern around each hole is different from each other due to the interaction. The mean flow with boundary layer enhances these changes.

The middle plots are the vertical slice in the middle of the two hole section which shows the perturbation inside the cavity and the effect on the acoustics of the liner unit when two holes line up in one direction. The plot in the right is another vertical slice in the middle of the one hole section which shows the wave pattern is different

from that of the two hole section. Inside the cavity, complex wave structures are observed near the holes. Near the bottom of the cavity (backplate), the waves become close to plane waves. It is believed that these wave structures will be very important for understanding the mechanism of liner aeroacoustics and to optimize their designs. In order to capture more detailed wave structures near the holes, more grid points and viscosity have to be used. Viscous effects have been included in the mean flow, but not in the perturbations. Outside the cavity, the influence from the boundary layer is clear.

To present more quantitative data, the peak of the sine wave is tracked. In fig. 14, three instantaneous acoustic pressure contour plots show the field when peak of the waves is above holes 1 to 3. At each of these times, the pressure perturbation along the center line of the hole is plotted in fig. 15. There is a pressure jump across the holes. The left side of this jump gives the pressure level inside the cavity and the right side shows the level in the duct. When the peak reaches the third hole, the pressure level has decreased in the duct, while the pressure level has increased in the cavity. The magnitude outside the cavity is much higher than that inside the cavity in these plots.

## Concluding Remarks

A better understanding of acoustic and aerodynamic mechanisms of engine liners is extremely important for optimizing liner design and noise prediction. For this purpose, a time domain method is applied to study the liner problem directly. In this paper a NLDE solver is developed based on the nonlinear disturbance equations along with the fourth order accurate method in space and time. Parallel computers (some of them are very low cost, e.g. a PC cluster) and a domain decomposition technique are used for the simulation of the engine liner model. This liner model is based on a test segment of the facility at NASA Langley. The code shows promise of time-accurate solutions of liner flow fields. It also shows that the NLDE is an approach to efficiently uncouple the low-speed mean flow from the acoustics. In future work, more fined grids around the holes will be used. The viscous effects on flow perturbations will also be considered. Eventually, the results will be compared with the experimental data from NASA Langley, in particular impedance data.

## Acknowledgments

We gratefully acknowledge the support and encouragement of T. Parrott, M. Jones and M. Tracy. This work was funded under the NASA grant NAG1-1833.

## References

- [1] Eversman, W., Parrett, A.V., Preisser, J.S., and Silcox, R.J., "Contributions to the finite element solution of the fan noise radiation problem", *Transactions of the ASME*, 107, 107, pp.216-223, 1985.
- [2] Hubbard, H.H., "Aeroacoustics of Flight Vehicles", V.1 and V.2., Published for the Acoustical Society of America through the American Institute of Physics, 1995.
- [3] Liu, J. and Long, L.N., "Higher Order Accurate Ship Airwake Predictions for the Helicopter/Ship Interface problem", *Proceedings of 54th Annual Forum of American Helicopter Society*, 1998.
- [4] Morris P.J., Long L.N., Bangalore A. and Wang Q., "A Parallel Three-Dimensional Computational Aeroacoustics Method Using Non-Linear Disturbance Equations", *J. Computational Physics*, Vol. 133, 1997.
- [5] Pacheco, P.S., "Parallel Programming with MPI," Morgan Kaufmann, San Fransisco, 1997
- [6] Krist, S.L., Biedron R.T., and Rumsey C.L., "CFL3D User's Manual (Version 5.0)," NASA Langley, Nov., 1996.
- [7] Ozyoruk Y. and Long L. N., "Time-Domain Impedance Boundary Conditions for Computational Aeroacoustics," *Journal of Computational Acoustics*, Vol. 5, No. 3, 1997.
- [8] Ozyoruk Y., Long L.N., and Jones M.G., "Time-Domain Numerical Simulation of a Flow-Impedance Tube," to appear *Journal of Computational Physics*, 1998.
- [9] Parrott, T.L., and Jones, M.G., "Experimental Validation of a Two-Dimensional Shear-Flow Model for Determining Acoustic Impedance", NASA Technical Paper 2679, 1987
- [10] Parrott, T.L., Abrahamson, A.L., and Jones, M.G., "Measured and Calculated Acoustic Attenuation Rate of Tuned Resonator Arrays for Two Surface Impedance Distribution Models with Flow. NASA TP-2766, January 1988.
- [11] Tam C.K.W., and Webb, J.C., "Dispersion-Relation-Preserving Finite Difference Schemes for Computational Aeroacoustics," *J. of Computational Physics*, Vol. 1, 1993.
- [12] Tam C.K.W., and Auriault, L., "Time-Domain Impedance Conditions for Computational Aeroacoustics", *AIAA Journal*, 34, No. 5, May, 1996.
- [13] Thompson K.W., "Time-Dependent Boundary Conditions for Hyperbolic System", *J. of Computational Physics*, Vol. 89, 1990.
- [14] Watson, W.R., Jones, M.G., Tanner, S.E., and Parrott, T.L., "Validating of a Numerical Method for Extracting Liner Impedance", *AIAA Journal*, 34, No. 5, 1996.
- [15] Watson, W.R., Jones, M.G., Tanner, S.E., and Parrott, T.L., "A Finite Element Propagation Model for Extrating Normal Incidence Impedance in Non-progressive Acoustic Wave Field", *Journal of Computational Physics*, Vol. 125, 1996.

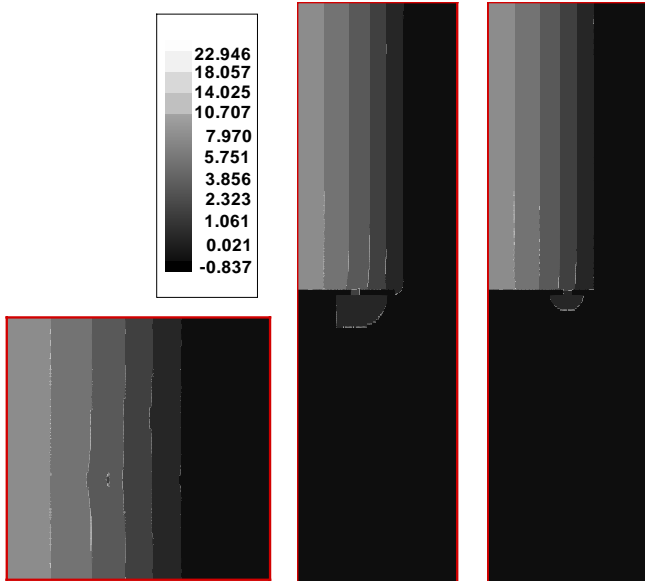


Figure 6: pressure perturbation at  $t = 0.1024T$  (without mean flow)

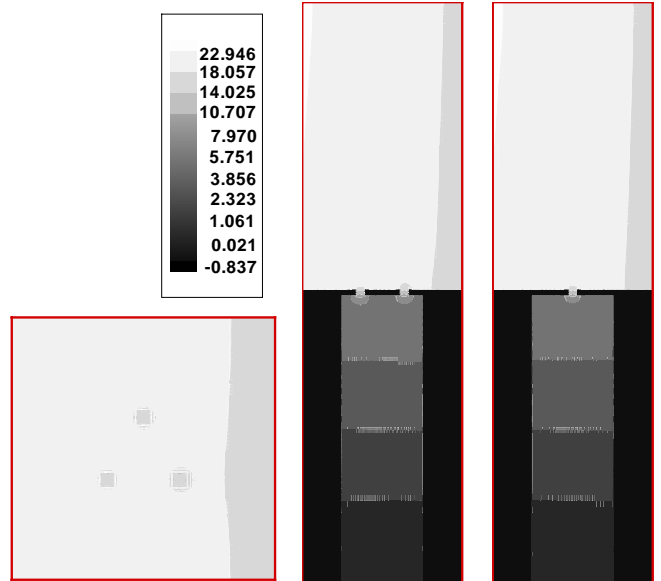


Figure 8: pressure perturbation at  $t = 0.4096T$  (without mean flow)

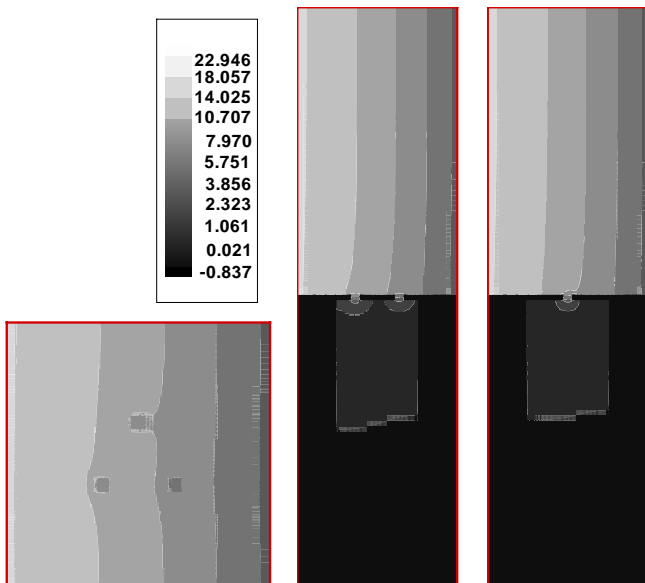


Figure 7: pressure perturbation at  $t = 0.2048T$  (without mean flow)

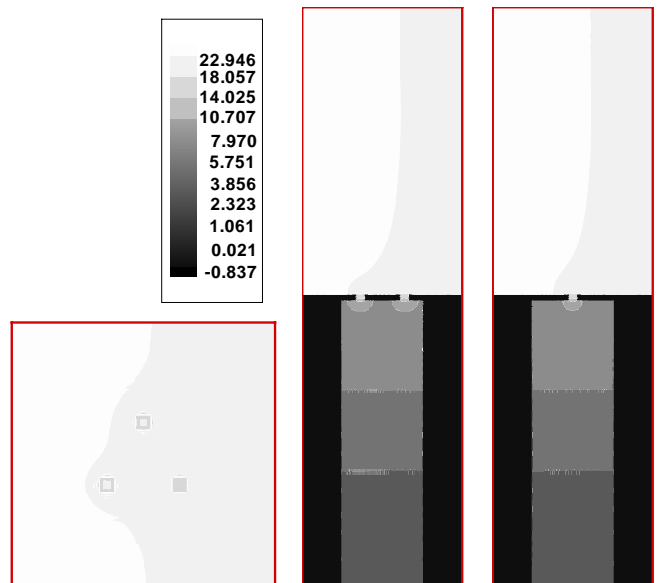


Figure 9: pressure perturbation at  $t = 0.5120T$  (without mean flow)

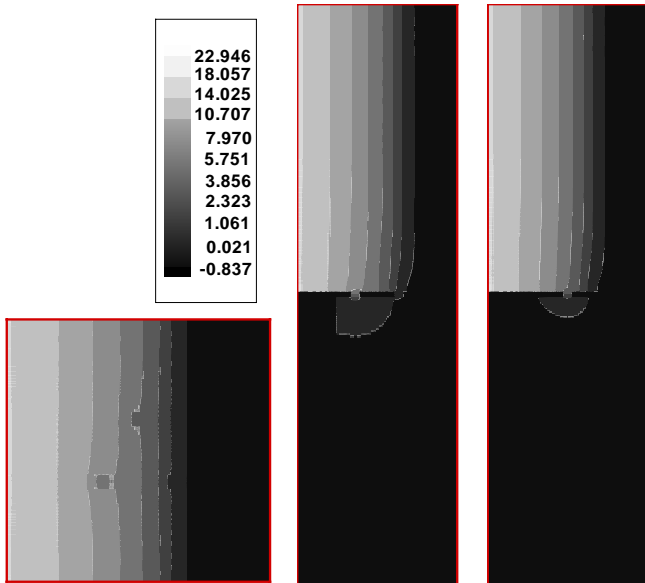


Figure 10: pressure perturbation at  $t = 0.1024T$  (with mean flow)

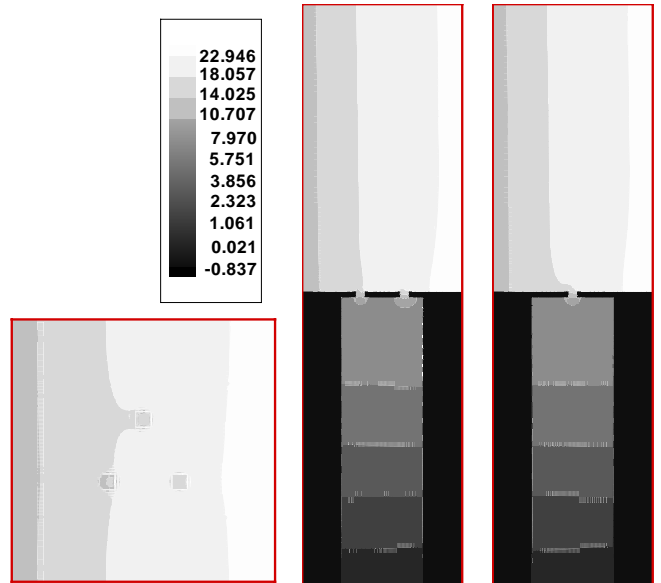


Figure 12: pressure perturbation at  $t = 0.4096T$  (with mean flow)

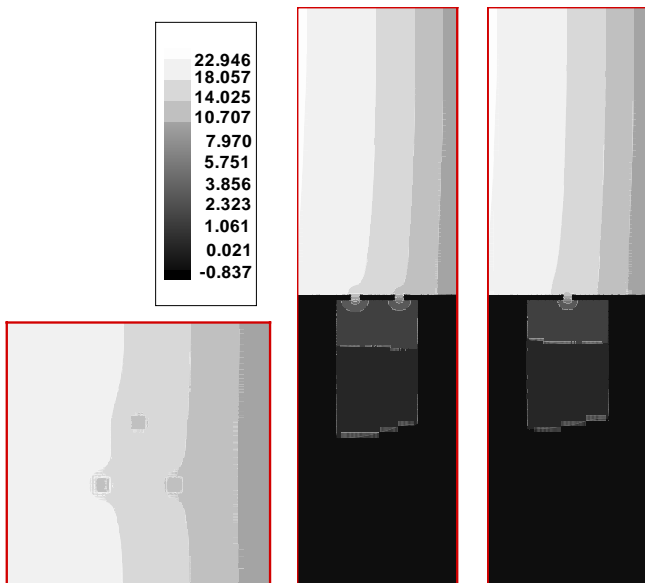


Figure 11: pressure perturbation at  $t = 0.2048T$  (with mean flow)

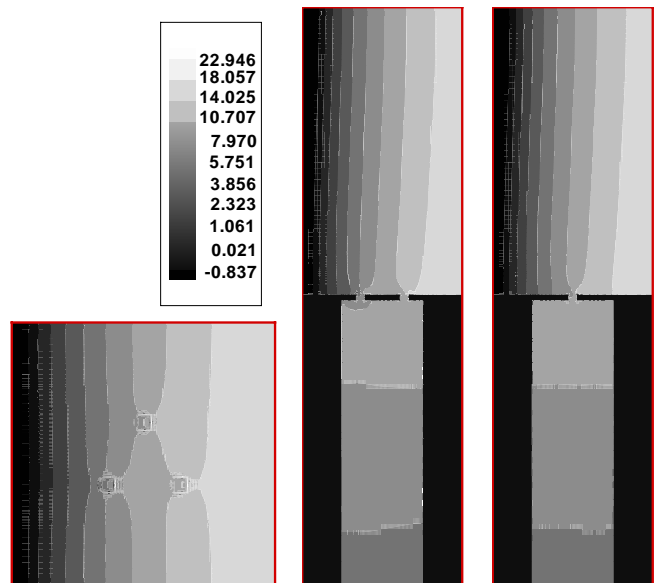


Figure 13: pressure perturbation at  $t = 0.5120T$  (with mean flow)

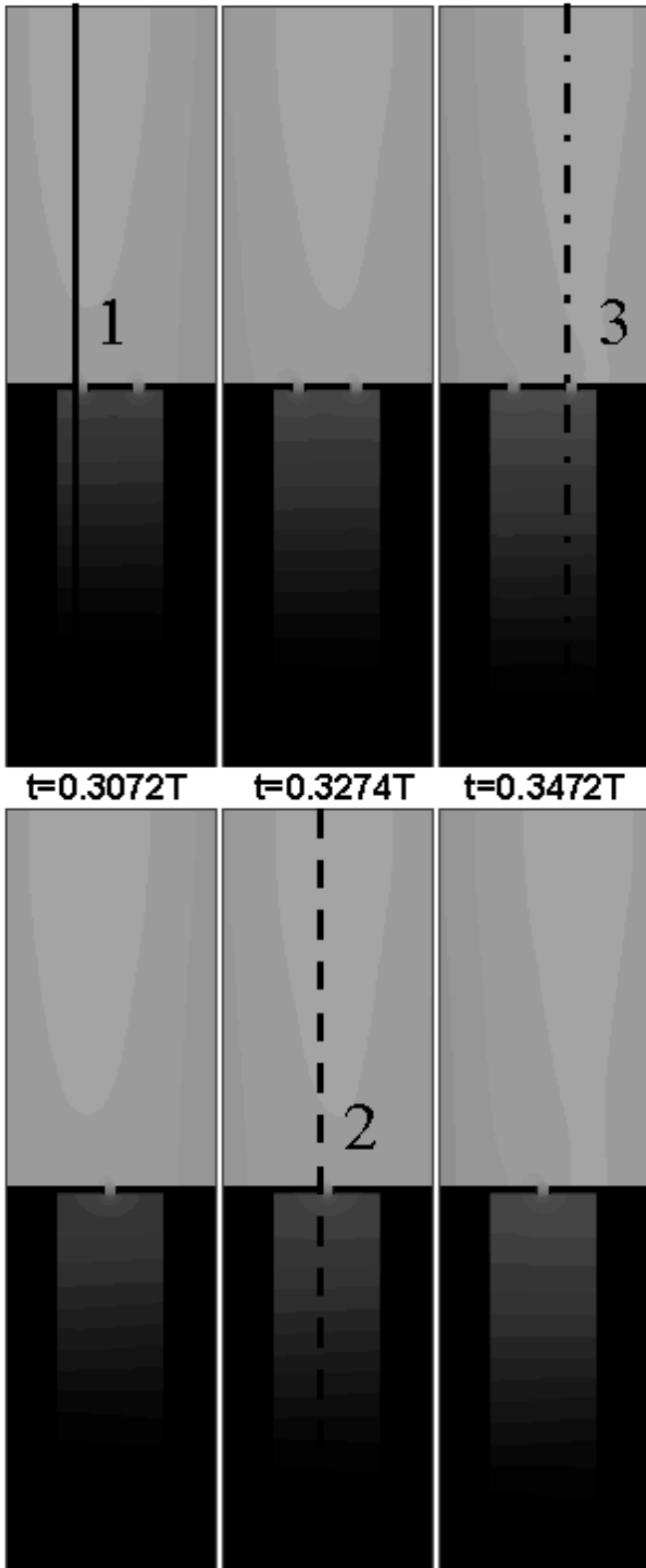


Figure 14: Wave peak moved from hole 1 to hole 3

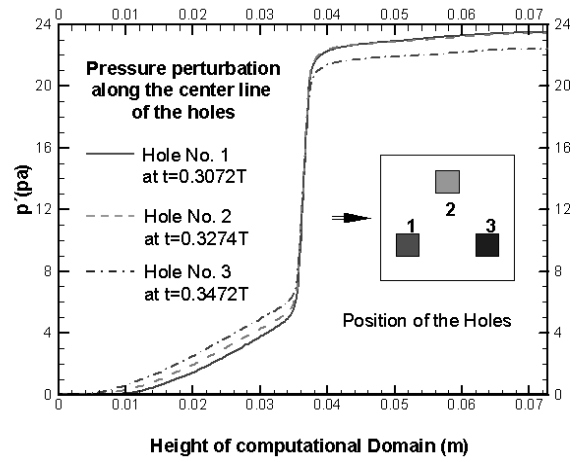


Figure 15: Pressure perturbation along the center line of the holes